In-orbit diagnostic of the EIT EUV CCD radiation induced aging.

Jean Marc Defise[a],
Frédéric Clette[b], John Daniel Moses[c], Jean-François Hochedez[d]
[1]and the EIT Consortium.

[a]Centre Spatial de Liège, Avenue Pré-Aily, B-4031 Angleur, Belgium
[b]Observatoire Royal de Belgique, Avenue Circulaire, B-1180 Bruxelles, Belgium
[c]Naval Research Laboratory, Washington, DC 20375
[d]Institut d'Astrophysique Spatiale, Universite Paris XI, F-91405 Orsay, France

ABSTRACT

The Extreme UV Imaging Telescope (EIT) on-board SOHO is performing a global survey of the extreme ultraviolet (EUV) solar corona. Operating since January 96, EIT has been producing tens thousands of images of the Sun in four narrow channels (171, 195, 284 and 304 Å). Orbiting around the L1 Lagrangian point and oriented permanently towards the Sun, the EIT mission is a unique opportunity to study an instrument continuously exposed to solar EUV radiations.
The backside thinned CCD detector is showing significant changes in its overall signal and in local "burn in" regions. Periodic bakeouts allowed to restore a good efficiency. However, a specific observation program has been set up to diagnose the origin of the signal decay. In this framework, photon transfer analyses are performed on solar EUV images, providing good indications on the local charge collection efficiency status. Calibration lamp images are also used to evaluate the signal recovery in the visible range.
The signal degradation seems to be the result of two competing effects: periodic deposition of a contamination layer, and charge mobility change in the CCD Si layer as a function of the accumulated EUV dose.
In this paper, the CCD quantum properties evolution is discussed, as well as the contamination issue. Preliminary diagnostics on the CCD aging under EUV radiations are exposed.

Keywords: EUV solar corona, CCD, radiation aging, contamination, photon transfer method.

1. INTRODUCTION

The EIT instrument is part of the SOHO payload, launched on 02-Dec-95 and orbiting around the L1 Lagrangian point since Feb-96. Permanently pointed towards the Sun, EIT [1] is imaging the solar corona in four EUV narrow bandpasses defined by multilayer coatings deposited on normal incidence optics: 171, 195, 284 and 304 Å. The images are produced on a 1024 x 1024 pixel CCD specially processed for EUV sensitivity enhancement. Each pixel of the detector is collecting the EUV radiation emitted by the solar corona in a 2.6 x 2.6 arcsec viewing angle. To fully achieve the scientific objectives of the instrument, it is mandatory to obtain a characterization of the overall sensitivity of the CCD, as well as relative sensitivities of all the individual pixels (flat fielding).
On-ground data were gathered during a complete calibration program [2]. These results allowed to obtain the exact definition of the bandpasses in order to analyze the contribution of individual solar emission lines with the flight data obtained during the mission. Overall photometric response and flat fields of the detector were also determined in view of the calibration of raw image data.
The EIT first light took place in early Jan-96, and an extensive synoptic observation program started in Feb-96. Despite a small light leak in one of the filters, the instrument is operating nominally, giving complete satisfaction to the scientific team [3]. However, monitoring the overall EUV solar signal recorded by EIT over a 2-month period revealed a significant

Authors informations
The EIT consortium and the authors e-mail addresses are detailed at http://umbra.nascom.nasa.gov/eit.

change in the EIT response. Applying a periodic baking sequence seemed a good recovery solution to release the potential contamination layer accumulated on the detector. But a detailed evaluation of the in-flight CCD response showed that local sensitivity changes were produced on several areas of the CCD, corresponding to highly EUV exposed regions. The laboratory flat field was thus subject to revision.
Therefore, efforts are put on the in-flight detector performance monitoring, in order to gather as much as possible informations on the CCD aging. These studies will hopefully provide adequate data to settle a diagnostic on the detector response variations, maintaining the quality of EIT scientific data the forthcoming years of the mission.

2. DETECTOR CONFIGURATION

The EIT detector is a thinned, back-illuminated CCD comprising an array of 1024 x 1024 square pixels. These features allow a high sensitivity in the EUV range.
The CCD chip is mounted at the end of a cold finger in a vacuum-tight compartment including the telescope elements (figure 1). The cold finger is conductively connected to a radiator viewing the cold space and some spacecraft parts. The design goal was a -80°C temperature at the level of the cold finger, in order to suppress most of the dark current, and limit the read noise to a few DN's. Keeping the detector at such a low temperature provides also an efficient way to overcome the effect of the silicon lattice defects which have trapped electrons.
The CCD can be heated above ambient temperature by a heater in its immediate proximity. This heating system was included in the design in order to evaporate any condensate that may have accumulated on the detector surface, and that would degrade the instrument response.
For stray-light rejection, the CCD is confined in a small volume defined by the vacuum housing and a stray-light baffle, equipped with a permanent aluminium filter, which blocks off the remaining unwanted radiations. Besides its very good stray-light performances, this configuration gives rise to a major drawback regarding the local environment of the instrument detector: the vacuum conductance out of the vicinity of the CCD is strongly reduced because it is restricted to 2 light labyrinths used for the visible calibration lamps. Therefore, a huge amount of time will be needed to evacuate all the gas and contaminant trapped within the CCD volume in the molecular pressure regime.

Contamination has been a concern since the beginning of the development of the instrument. The extreme sensitivity of the EUV transmission to the organic components requires very strict cleanliness conditions. Moreover, as the CCD is one of the coldest surface (-80°C) inside the instrument while the vacuum housing remains near 20°C, condensed gas and contaminants were expected on the detector surface. Therefore, before SOHO's launch, the EIT instrument was kept under internal vacuum (lower than 10 mbars), to ensure cleanliness and overpressure safety of the thin aluminium filters used to reject visible light. This care would limit the contaminants in the CCD surroundings, reducing then the potential condensable materials.

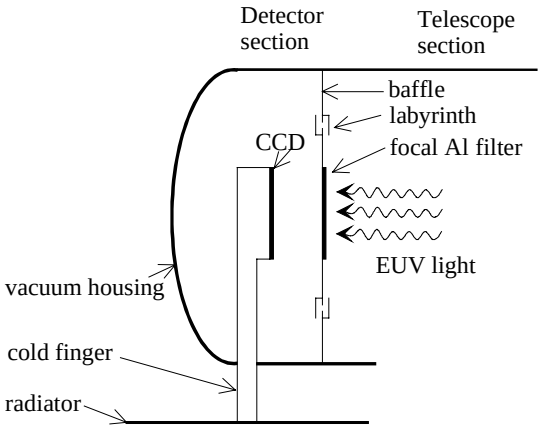

Figure 1: Configuration of the detector section.

3. EIT FIRST OPERATIONS

Launched on 2 Dec 95 from KSC, EIT was vented just one week later during the orbital transfer phase. The spacecraft has already reached its final attitude towards the sun, allowing the radiator to cool down. The telemetry indicated that the CCD was still at -53°C, far above the target temperature of -80°C. After a 2 week CCD bakeout period, the continuous monitoring of the CCD temperature sensor indicated a slow cooling trend, while SOHO was keeping its attitude constant. This initial warm status could be attributed to a relatively high residual pressure inside the detector section, due to the inefficient vacuum pumping capability of the camera section and progressive outgassing of the inner surfaces. Gas remaining in the section

produces thermal leaks, thereby reducing the cooling effect of the cold finger. The subsequent steady cooling then followed the slow pumping of the CCD cavity.

After several weeks, the final CCD temperature reached -67°C. In these conditions, the dark current remains lower than a single DN, providing excellent CCD performances. This temperature evolution shows that the CCD volume was not exempt from trapped gas and that condensates were present on the coldest surfaces. Humidity in the ambient air of the clean room where the instrument was integrated can be one of the main contributors to this residual condensables, inducing ice accumulation on the cold surfaces.
The scientific operations started in Jan 96, EIT began producing several tens of EUV images every days.

4. EUV CONTAMINATION ISSUE

After several weeks of operations, it became possible to build a curve of the total response of the CCD versus time. In early 96, the solar activity was at its minimum level. Therefore, the sun showed only small flux variations in 2 of the 4 channels, and long term variations of the integrated signal can be reasonably attributed to a change in the instrument response. After a steady increase of the response during the first month, a continuous decline in the total response (total count / s) was observed. Analyzing the 304 Å channel, which shows the largest variations, the initial 70 % rise can be related to the progressive de-icing of the CCD, obtained after a long pumping period and to general outgassing of all the optical surfaces. Then, EIT was switched to its normal operating mode, in which the detector started accumulating new condensables on its surface. This continuous deposition of molecular layers on the CCD can have a drastic effect on the EUV detection function of the pixels. The degradation rate of the response is of the order of 10 % per month. The presence of residual atmosphere in the instrument at launch time let us infer that water vapor is the main contaminant on board EIT, as great care was taken to avoid other potential contaminating materials. Using Henke [4] scattering factors to compute the complex refractive index of the ice, the transmission drop as a function of the ice layer thickness can be calculated for normal incidence (figure 2).

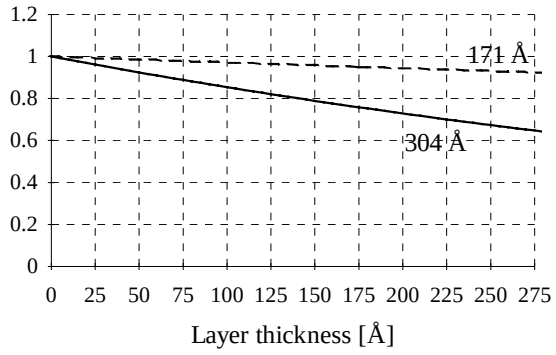

Figure 2: Transmission of an ice layer at 304 and 171 Å

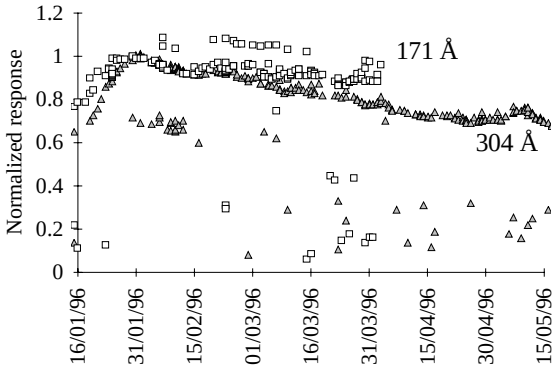

Figure 3: Total response at 304 and 171 Å

Figure 3 illustrates the response degradation at 304 Å starting in early Feb 96. The response at 171 Å is partly dominated by solar variations which are larger in that channel. However, the downwards trend is also observed. Referring to the transmission of an ice layer as a function of its thickness, it appears that the 171 Å is less affected by this kind of contaminant than the 304 Å lower energetic radiation. A loss of 10 % per month at 304 Å corresponds to a 70 Å deposit of ice. The monthly loss at 171 Å corresponding to this ice deposition rate amounts to only 2 %, which is barely detectable out of the solar noise affecting the response plot, but the order of magnitude seems to be in rough agreement.

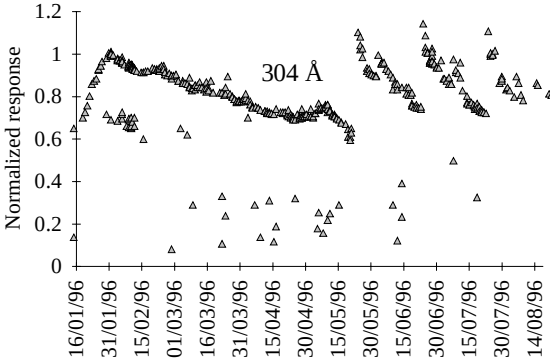

To counteract this response degradation, a recovery program was set up. Periodic bakeouts of the detector have been conducted using the decontamination heater, in order to release periodically the condensed material from the cold finger and the CCD. The bakeout effect is immediate. By heating from -67°C to +15°C for a few hours, the response is fully restored. Figure 4 shows the effect of the first three bakeouts (45 hours end May-96, 24 hours end Jun-96 and 2.5 hours end Jul-96), which brought temporarily the response beyond the first maximum of early Feb-96.

The bakeout duration does not seem to influence the amount of improvement. Unfortunately, the contaminants released by the first bakeout remain confined in the camera section, and accumulate again on the cold surfaces, at a rate that seems to be higher than for the first four operational months preceding the first bakeout. However the response still falls off exponentially in agreement with a constant rate contaminant deposition.

5. EUV RADIATION DAMAGES

An instrument malfunction occurred on July 27, and left the shutter open for 7 hours in the 304 Å channel. As a result of this failure, a burned in blemish appeared on the CCD at the location of a bright active region. Figure 5 shows the first 304 Å image taken after this event. The main burn-in feature is marked by the white square area, and the responsible active region had then rotated towards the center of the solar disk. This was the first clear example of a non-uniform damage affecting the detector. A local response loss of 90 % was recorded in the burn-in region at 304 Å, and of around 60 % in the other 3 channels. Moreover, a 20 % drop of the total 304 Å response was also detected, suggesting that a large portion of the sensor area was affected by this EUV over-exposure.

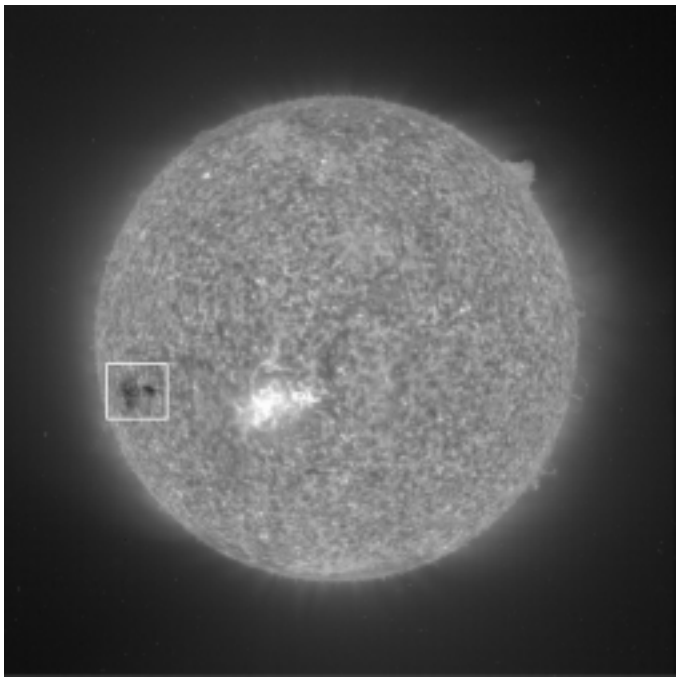

Figure 5: Image of the solar corona just after the shutter incident (304 Å).

The subsequent progress of this CCD degradation was carefully analyzed. We quickly verified that it occurs inside the detector structure, and is not a surface effect, like a contaminant layer. The CCD quantum properties are directly degraded by this EUV overdose.
In order to diagnose the detector degradation, statistical analyses on the solar images were carried out. The photon transfer method (Jannesick [5]) is used to characterize the charge collection efficiency (*CCE*), i.e. the collected electrons per interacting photon, in the EUV range.

$CCE = \frac{\eta_E}{\eta_i}$, with η_i and η_E being the ideal and the effective quantum yields

$\eta_i = \frac{E_\lambda}{3.65}$ (λ < 1000 Å) is the theoretical number of generated electrons per photon of energy E_λ (eV)

η_E is the average number of collected e- per pixel receiving an interactive photon.

An ideal CCD would have $\eta_E = \eta_i$ and a unit CCE. In a real device, there are less collected electrons in each pixel, due to recombination of charges before collection (traps in the Si) and charge splitting over several pixels. The EUV measured CCE was close to 30 % during ground-based testing.
An indirect evaluation method of the evolution of η_E can give precious indications about the CCE variations. This can be achieved by measuring the ratio of K, the signal gain (e-/DN), with J, the number of interactive photons/DN. The photon transfer (PT) method identifies J^{-1} as the slope of the photon shot noise versus the signal, in the EUV range, while K^{-1} is the slope of the corresponding plot with photons in the visible wavelength range.

$\eta_E = K/J$

K depends only on the electronics and should not vary since its on-ground determination. Its measured value [2] was close to 15 e-/DN.

By analyzing subfield images of the Sun acquired at high temporal cadences, intrinsic solar variations are reduced to a minimum, and are dominated by the shot noise, in the 171 Å channel. The subframe mode is required to achieve the high cadence acquisition. Figure 7 shows a photon transfer curve computed for a subframe centered on the active region blemish, taken just after the shutter failure, in early Aug-96 (figure 6). Zone 1 is a "quiet" area, outside the solar disk, zone 2 is the burn-in defect, and zone 3 is covering a "quite" area, solar limb, and in-disk regions where no apparent burn-in occurred.

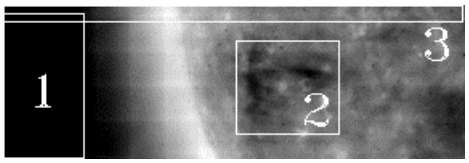

Figure 6: The subframe used for PT analysis

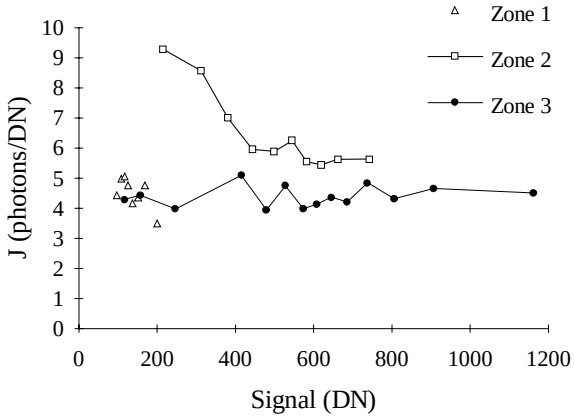

Figure 7: Results of the PT analysis at 171 Å

Figure 7 reveals a clear change in the CCE inside the burn-in region. While zone 1 and 3 share very similar J values, whatever the signal level, the burn-in (zone 2) shows a strong dependency of the J parameter with the signal value: the number of EUV photons/DN decreases as the signal decreases. The dark pixels in zone 2 are thus the pixels most affected by the EUV damage. This demonstrates that the apparent drop of the local sensitivity is due to a reduction of the CCE, and not simply to absorption by a local contaminant deposit or polymerization.

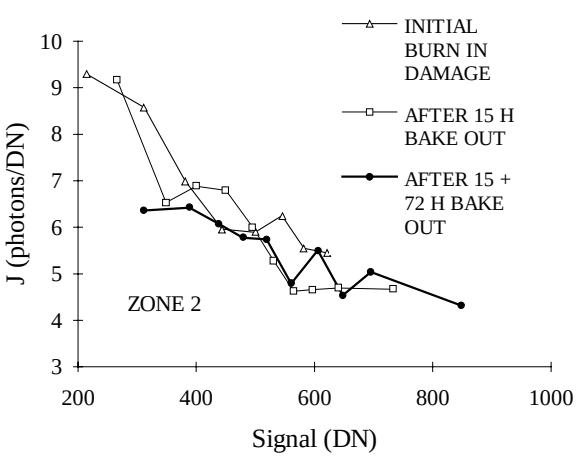

Figure 8: Bakeout effect on the EUV damage (171 Å)

Heating up the CCD to ambient temperature produces an annealing effect on the radiation damage. Specific PT observation sequences covering zone 2 of the same subframe (figure 6) were taken just before and after the forthcoming bakeouts. An improvement in the CCE can be detected, as shown in figure 8.

The bakeout effect, as shown in figure 8, is positive in terms of CCE recovery. The curves are shifted toward the higher signal level, showing an apparent recovery, and the J parameter is decreasing. The recovery after 2 bakeouts is far from being complete, but good progress can be obtained with this warm-up procedure.

˝

The SOHO pointing remains remarkably stable and was left almost unchanged since the beginning of the mission, the solar disk and the solar limb are irradiating a constant region on the detector. The solar rotation carries the active regions from west to east mainly along two low latitude belts. When a map of the EUV accumulated dose on each pixel is built, it shows the potential regions where the CCE could be affected by high EUV dose.

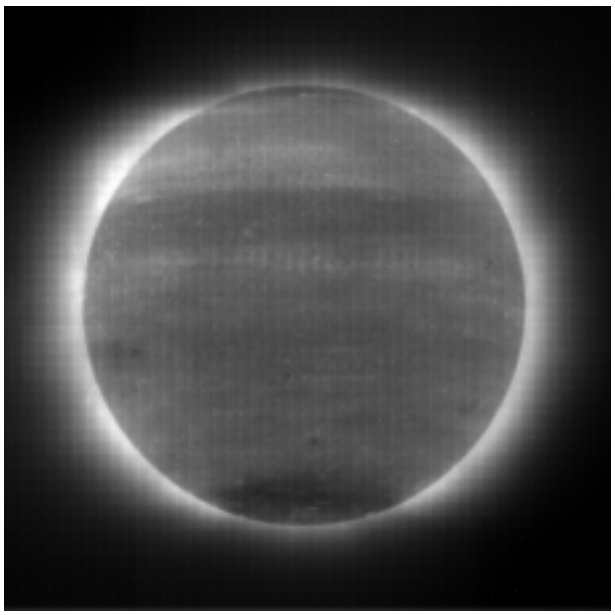

Figure 9: Total accumulated 195 Å signal (in Feb-Mar 97)

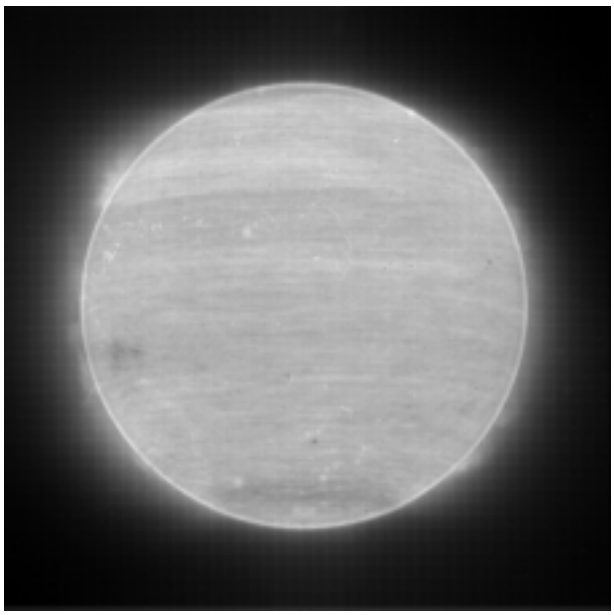

Figure 10: Total accumulated 304 Å signal (in Feb-Mar 97)

Figure 9 and 10 show maps of the total accumulated EUV dose at 195 and 304 Å over a 12 day period, from Feb 21, 1997 bakeout to Mar 4, 1997. These two channels show very different dose patterns, due to the different natures of the solar emission lines and also to the specific observation plans for each channel. The 304 Å channel (He II) is illuminating mainly the solar disk, with local in-disk features, while the main emission of the 3 iron coronal lines (171, 195 and 284 Å) are located along the solar limb and show similar properties. Each channel is also affected by the imprint of a specific grid pattern due to aluminium filter supports.

If we use these maps to define high dose regions, we can infer that the EUV damage of the CCD is mainly due to the 304 Å high emission. Local CCE degradation can be evaluated on different high dose regions. A subfield image sequence localized across the east limb (figure 13) has been used to compute the J parameter (photons /DN) in the EUV range. Three different regions in this subfield image were used to conduct PT analysis. As shown in figure 11 and 12, region A is a high 304 Å dose area with medium 195 Å dose, region B is a high 195 Å dose area with medium/low 304 Å dose and region C is kept far from all EUV high irradiation.

Figure 14 shows that the CCE is reduced in high 304 Å dose regions (A), while unchanged in high 195 and low 304 Å dose regions (B) as well as in low signal area (C). However this diagnostic tool based on solar images has its own limitations, and remains now a qualitative approach to identify the CCE damage. The solar noise is affecting the collected data, even at high temporal rate. These results can be obtained mainly with the 171 Å channel. The other channels do not seem to allow a reliable PT analysis due to the presence of high solar noise or to their longer exposure time.

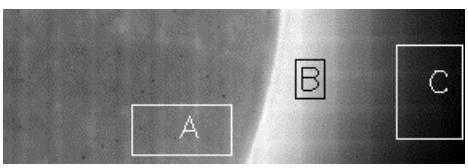

Figure 11: Total 195 Å signal in a subfield of fig. 9

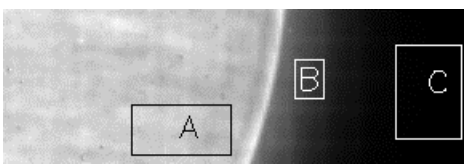

Figure 12: Total 304 Å signal in a subfield of fig. 10

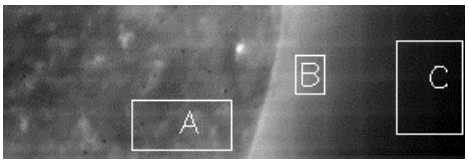

Figure 13: 171 Å subfield image taken at high temporal cadence on 04-Mar-97

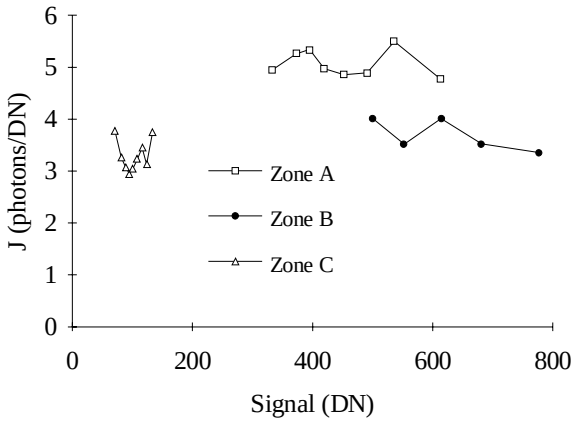

Figure 14 (right): Result of the PT analysis in regions A, B & C.

A physical explanation can be advanced concerning the nature of the damaging processes occurring in the CCD structure. The EIT CCD is exposed to very high EUV irradiation levels, quite uncommon during on-ground testing, and is permanently maintained at very low temperatures. These sustained exposures to radiation in a stable cold environment lead to the cumulative charging of the SiO_2 front layer by photoelectric effect. Electrons are generated by energetic EUV photons in the surrounding field-free regions, where the charge mobility is very low. As illustrated in figure 15, this creates a dipolar layer directly at the oxide layer interface, generating a local electric field. The extent of the electric field is growing with the continuous ionization of the SiO_2. Therefore, a trapping region is created and can affect the collection efficiency in the affected pixels.

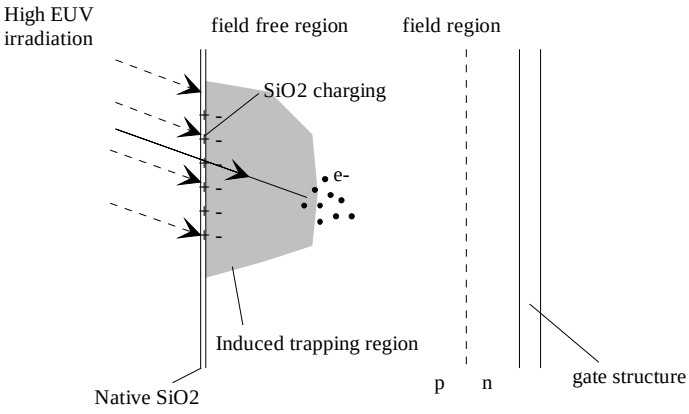

Figure 15: Generation of EUV-induced traps in the backside CCD

During the bakeout sequences, the thermal agitation induces a self-annealing effect. A complete restoration can be reached only if all the charges of the SiO_2 layers have been redistributed and the traps suppressed. This process can take a very long time and can explain the impact of the bakeout duration on the CCE improvement process. This kind of damage is not commonly seen during laboratory testing of EUV CCD's, due to the need of high EUV dose and to the self annealing occurring during thermal cycles applied to the detectors.

The EUV local degradation of the CCE is mainly due to the 304 Å irradiation. This can be explained by the fact that the CCE decrease is produced by native oxide layer ionization. The 304 Å radiation is the one having the smallest penetration depth among the 4 channels of EIT. Therefore, the 304 Å photons will interact with the first layers of the CCD structure, as a matter of fact with the external oxide layer. The 284 Å photons have a similar penetration depth, but their low exposure level is not a real concern for the CCD degradation. The low global exposition of the CCD to 284 Å is explained by the following reasons:

- the 284 Å solar emission is lower than the 304 Å
- even with long integration times, the 284 images have a lower global signal, as the peaks are located in concentrated bright points
- the time scale of the 304 Å solar events is smaller than the 284 Å events, and requires repetitive observing sequences (typically 50 images/week), while the 284 Å channel produces only one or two daily images.

6. CCD RESPONSE IN THE VISIBLE

The CCD sensor can be indirectly illuminated by a calibration lamp producing visible and near-infrared light. This device is very useful to monitor the evolution of the detector response. Therefore, calibration lamp images are made on a regular basis, in particular just before and after sensor bakeouts. Several diagnostics can be derived from these images :

- spatial variations in the evolution of the visible response, i.e. changes in the visible-light flatfield
- global restoration effect of bakeouts
- photon transfer analysis to determine the signal gain at visible wavelengths (K)

6.1.a Evolution of the visible-light flatfield

Calibration lamp images show that the steady degradation of the response and its partial restoration by bakeouts are also observed in visible light (figure 17). Thanks to the good stability of the illumination, clean images of the spatial distribution of the degradation can be obtained (figure 16). However, the amplitude of the degradation is lower in the visible than in the EUV, and the EUV/visible ratio changes according to the location on the CCD. For instance, the contrast of the "active region" burn-in blemish relative to the average disk level is much higher in the EUV than at longer wavelengths (ratio = 8), while the average signal loss on the disk is more similar in both wavelength ranges (ratio= 1.5). The amount of recovery after a bakeout also displays local variations : the dark core of the "active region" blemish tends to fade more quickly in calibration lamp images than in the EUV images, after successive bakeouts.

The above differences again confirm the presence of different degradation mechanisms, which contribute in varying proportions according to the nature of the local irradiation : steady low-level irradiation (quiet solar disc) or strong short-lived light pulses over small areas (loop brightenings, flares). Finally, the low level of degradation observed off the limb relative to the disc, as well as the coincidence of the inverted grid image with the 304 Angstrom grid pattern, both indicate that this latter waveband contributes for a large part to the total radiation damage.

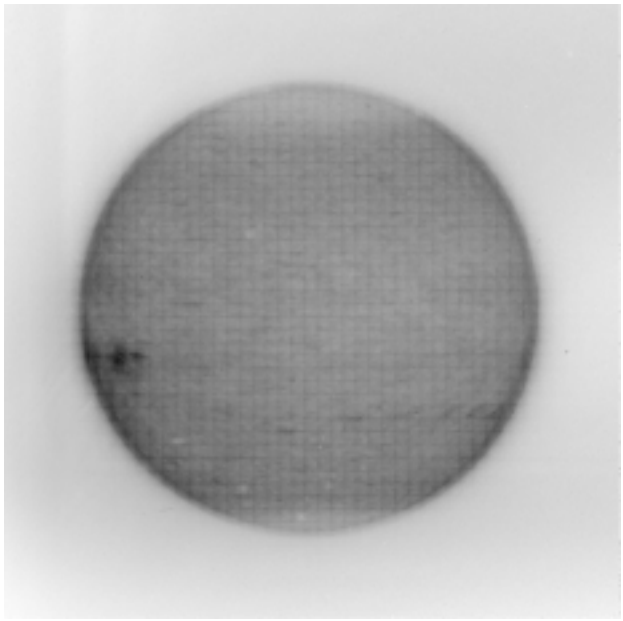

Figure 16 (right): Spatial distribution of the radiation damage derived from calibration images (January 3,1997). The degradation of the response is largest on the disc, where the imprint of individual solar features (e.g. the July 29 burn-in) and the modulation of the 304 Å grid pattern of the aluminium focal filter (figure 1) of the can be recognized.

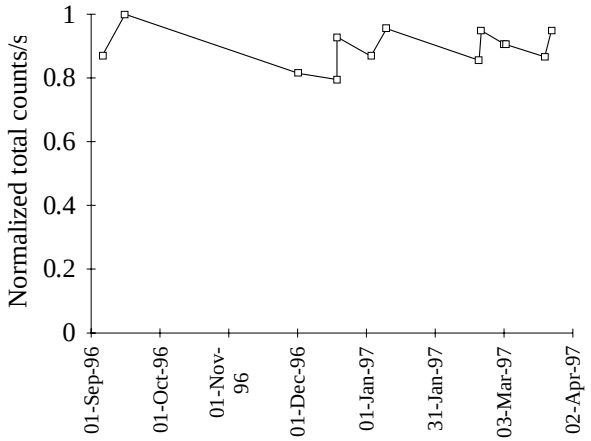

Figure 17 (left): The total response is affected after long periods with the CCD kept at -70°C. After analyses of visible images taken before and after each decontamination phase, we can infer that most of the decrease of the total visible response is restored after the bakeout sequence.
This figure relates the total response of calibration lamp images before and after 5 bakeout sequences.

6.1.b Signal gain verification

Statistical analysis of the noise can be carried out using pairs of calibration lamp images. At visible wavelengths, the gain (e-/DN) can be evaluated with the PT method (section 4). As expected, we did not find any change from the on-ground measurements.

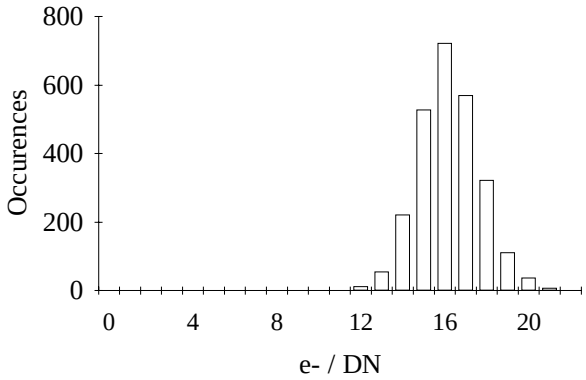

Figure 18: The gain can be evaluated by plotting a transfer photon histogram, including all the gain values computed on small subframes (i.e. 50 x 50) covering all the detector area. As shown in this figure, the central value is very close to the 15 e-/DN pre-flight measurement [2]. Moreover, the spatial distribution in all the subframes remains very homogeneous, without any influence of the solar disk imprint in the visible calibration lamp images.

6.2 Visible-light leak

The 284 Å images are affected by a local light leak on the northern edge of the field. This leak can be completely suppressed by the adjunction of an additional aluminium filter available in the filter wheel, but increasing the exposure time. The concentrated light leak is probably produced by the combination of pin holes in the 284 Å entrance aluminium filter and a tear in the focal aluminium filter resulting from the SOHO launch. A faint similar leak can be detected at the same location in the 171 Å images.

The PT analysis can be used to characterize the solar photons producing the light leak. With a subfield high cadence sequence centered on the light leak area, the photon shot noise distribution lead to evaluate the K (e-/DN) or the J (photons/DN) parameter. If EUV photons are producing the leak, the noise slope will identify photons/DN, but if wavelengths higher than 3000 Å are present, the slope will identify the gain value (electrons/DN). As shown in figure 20, a value close to 16 is obtained. It is very close to the gain (K) measured with calibration lamp, and it remains far from the J value roughly evaluated by solar PT analysis at 304 Å, around 7 photons /DN. Therefore we have shown evidence that the leak is constituted of visible light.

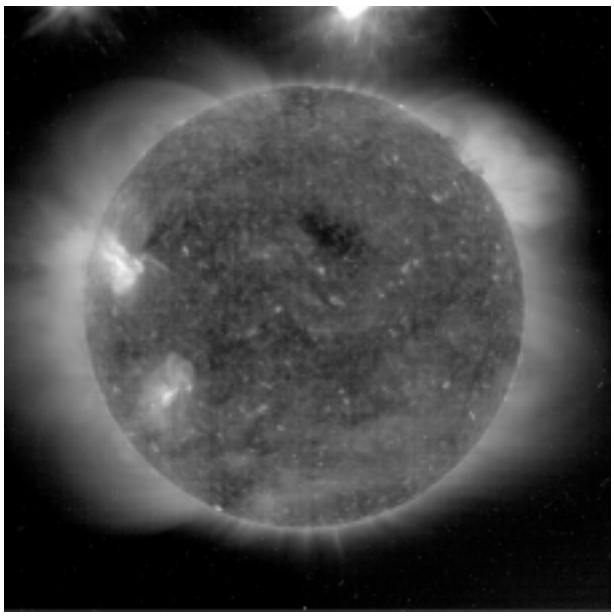

Figure 19 (left): Solar image in the 284 Å channel, with light leaks on the northern border of the field

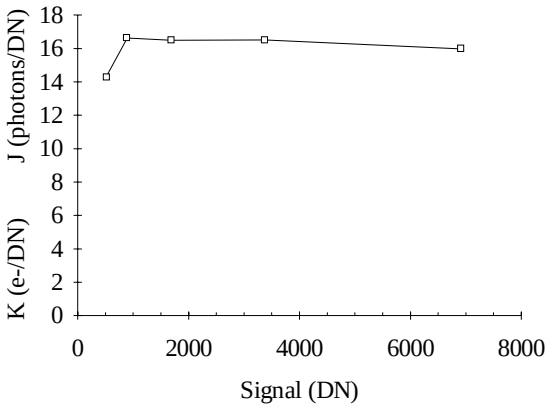

Figure 20 (above): Result of the PT analysis in the light leak region

7. CONCLUSIONS

The evolution of the EIT response during its long cumulative exposure to solar EUV radiation can be explained by two competing effects: the periodic deposition of a contaminant layer and the local change of the CCD charge collection efficiency. They both induce a response decay. Properties of both damaging processes are summarized in the table 1.

CONTAMINATION	EUV DAMAGE
Global effect on the whole CCD surface	Local effect
Fast bakeout recovery	Very slow and variable bakeout recovery
CCE efficiency is unaffected No EUV dose effect	CCE efficiency is decreased Dependant on the local accumulated EUV dose

Table 1: Comparison of the 2 in-flight response degradation processes of the EIT detector.

A maintenance program has been included in the EIT operation schedule in order to monitor the detector changes, to evaluate the sensitivity and the spatial uniformity of the response. In-flight flat-field maps need to be regularly evaluated to cope with the local variations of the instrument response. Global changes affecting the overall require also specific attention.

This can only be obtained by a permanent monitoring of the instrument response (overall response, accumulated radiation dose and corresponding local changes), that will be pursued until the end of the mission. Operational constrains will be derived from these monitoring sequences, in order to prevent excessive or unrecoverable damages to the EIT detector.

Further analyses are undertaken to improve our understanding of the mechanisms affecting detector performances, such as the possible EUV polymerization of the condensed contaminants. Moreover, the EIT Calroc sounding rocket experiment, to be flown in the forthcoming months, will provide new data with a similar instrument to perform a recalibration of the SOHO-EIT response.

ACKNOWLEDGMENTS

This program was developed in the frame of the Science Program of ESA with support from Belgian SSTC, NASA and CNES.

REFERENCES

1. Delaboudinière et al., "EIT: Extreme-UV imaging telescope for the SOHO mission", Dec 95, Solar Physics, Vol 162 n°1-2.
2. J.M. Defise, J.P. Delaboudinière et al, R.C. Catura, F. Clette, A.J. Maucherat, "Calibration of the EIT Instrument", 1995, SPIE Vol. 2517, pp 29-39.
3. Moses et al., "EIT Observations of the Extreme Ultraviolet Sun", 1997, accepted for publication in Solar Physics.
4. B.L. Henke, E.M. Gullikson and J.C. Davis, "X-ray interactions: photoabsorption, scattering, transmission and reflection at E=50-30000 eV, Z=1-92". Atomic Data and Nuclear Data Tables, Vol 54, N°2 (1993).
5. Jannesick J.R., Klaasen K.P., Eliott T., Oct-87, Optical Engineering, 26, N°10.